THE JOURNAL OF PHYSICAL CHEMISTRY C

Article

pubs.acs.org/JPCC

Insights into Bulk Electrolyte Effects on the Operative Voltage of Electrochemical Double-Layer Capacitors

Promit Ray,[†] Sebastian Dohm,[‡] Tamara Husch,[‡] Christoph Schütter,[§] Kristin A. Persson,[∥] Andrea Balducci,[§] Barbara Kirchner,[†] and Martin Korth*[,‡]

[†]Mulliken Center for Theoretical Chemistry, Rheinische Friedrich-Wilhelms-Universität Bonn, Beringstr. 4 + 6, D-53115 Bonn, Germany

[‡]Institute for Theoretical Chemistry, Ulm University, Albert-Einstein-Allee 11, D-89069 Ulm, Germany

[§]Helmholtz Institute Ulm, Karlsruhe Institute of Technology, Helmholtzstraße 11, 89081 Ulm, Germany

[∥]Electrochemical Technologies Group, Lawrence Berkeley National Laboratory, 1 Cyclotron Road MS 33R0146, Berkeley, California 94720, United States

Supporting Information

ABSTRACT: Electrochemical double-layer capacitors (EDLCs) are robust, high-power, and fast-charging energy storage devices. Rational design of novel electrolyte materials could further improve the performance of EDLCs. Computational methods offer immense scope in aiding the development of such materials. Trends in experimentally observed operative voltages nevertheless remain difficult to predict and understand. We discuss here the intriguing case of adiponitrile (ADN) versus 2-methyl-glutaronitrile (2MGN) based electrolytes, which result in very different operative voltages in EDLCs despite structural similarity. As a preliminary step, bulk electrolyte effects on electrochemical stability are investigated by *ab initio* molecular dynamics (AIMD) and static, cluster-based quantum chemistry calculations.

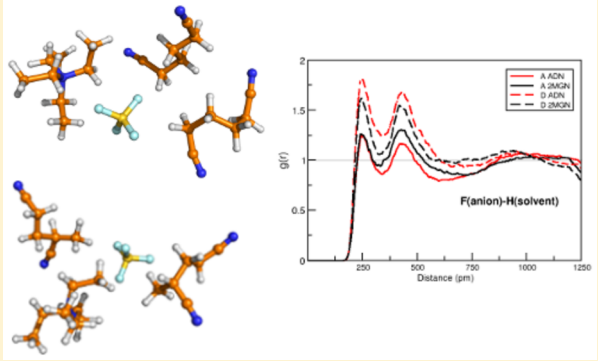

1. INTRODUCTION

Supercapacitors or electrochemical double-layer capacitors (EDLCs) store charge at the interface between the electrodes and the electrolytes, allowing for very high cycle life, high power, and fast charging.[1−4] Therefore, they are considered as devices of choice for a number of energy storage applications, and improvement in the design of EDLCs is seen as extremely promising within many future energy strategies. The biggest impact could be achieved by the introduction of new materials as alternatives to activated carbon electrodes and organic solvent based electrolytes.[5−8] Considerable academic interest is currently devoted to increasing the operative voltage, currently limited to about 2.7 V by the commonly used acetonitrile (ACN) or propylene carbonate (PC) based electrolytes. Further research on EDLCs electrolytes is, therefore, of central importance for the development of improved devices, especially because we still lack atom-scale knowledge of factors determining operative voltage.

We have recently reported the development of innovative electrolytes for EDLCs based on an integrated computational and experimental screening strategy.[9] Within this approach, computational methods at different levels were systematically applied to preselect candidates for subsequent experiments. Applying this computational screening to "toy systems" of all reasonable nitrile solvents with up to 12 heavy atoms, several promising candidates were identified. Experimental validation, of these previously unexplored yet commercially available solvents, showed that our scheme is indeed a feasible strategy to "rationalize" the design of new electrolyte materials.

However, it was also found that predicting trends in operative voltages could be rather challenging; while the trend of the electrochemical stability of the electrolyte solutions themselves was predicted in good agreement with subsequent experimental measurements, very different operative voltages were found for their application in EDLC devices. Apart from the previously investigated ACN and adiponitrile (ADN), two "new" solvents, glutaronitrile (GTN) and 2-methyl-glutaronitrile (2MGN), were also investigated. While ADN, GTN, and 2MGN show rather similar operative voltages, ADN-based electrolytes allow for a value almost 1 V higher. As all other conditions (electrodes, salt, etc.) were kept the same and the electrolytes themselves (solvent plus salt) showed very similar electrochemical stability windows, it seems clear that the increased stability must be addressed to the specific interaction between solvent and salt and the interplay of this interaction with the electrodes.

Received: January 27, 2016
Revised: May 12, 2016
Published: May 23, 2016

DOI: 10.1021/acs.jpcc.6b00891
J. Phys. Chem. C 2016, 120, 12325−12336

We have recently found that the operative voltage of EDLCs with PC-based electrolytes can be influenced by changing the conductive salt.[3] Therefore, as a first step, it is important to investigate possible consequences of salt--solvent interactions on the operative voltages. In the following, we focus on comparing electrolytes based on ADN and 2MGN, as these two solvents are structurally similar isomers but show very different operative voltages in EDLCs with active carbon (AC) electrodes and tetraethylammonium tetrafluoroborate (Et_4NBF_4) salt. The structures of the two solvents are given in Figure 1. The experimentally found electrochemical stability

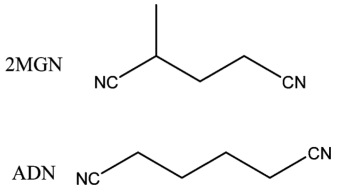

Figure 1. Lewis structures of the two nitrile solvents investigated.

windows of the pure electrolytes (solvent plus salt) are practically identical, about −1.8 V (−1.75 for 2MGN, −1.85 V for ADN) to +3.7 V against Ag/Ag+, which indicates that these limits are probably imposed by the stability of the conductive salt Et_4NBF_4. The operative voltage of EDLC devices with ADN versus 2MGN can be measured, from the three-electrode setup CV measurements depicted in Figure 2, to be 3.7 V (−1.85 to +1.85 V) for ADN but only 2.95 V (−1.90 to +1.05) for 2MGN. It is this surprising observation we try to address here, with an investigation into the corresponding properties of each of the electrolytes.

Our experimental findings suggest that differences in operative voltages will be related to changes in bulk electrolyte features at the electrode interface, consistent with recent findings by Griffin et al.;[10] using *in situ* NMR and electrochemical quartz crystal microbalance measurements, they revealed that the charging mechanism of microporous carbon based EDLCs is based on different processes at the positively and negatively polarized electrodes. At least, in the case of Et_4NBF_4 in ACN, an exchange of cations with anions is observed for the positively polarized electrode, while cation adsorption dominates at the negatively polarized one. Also, recently, the effect of strong ion pairing in Mg electrolytes[11] was found to significantly impact the stability of the electrolyte, e.g., the operative voltage window. As partial desolvation and possible ion pair formation play a central role in both cases, it appears imperative to understand differences between ADN versus 2MGN based bulk electrolytes.

2. THEORETICAL CONSIDERATIONS

ADN and 2MGN were selected as electrolyte solvents among several promising candidates by a computational screening approach developed recently,[12] which takes into account electrochemical stabilities (IPs/EAs), melting/flash/boiling points, viscosities, and ion solubilities,[13] with density functional theory (DFT), semiempirical quantum mechanical (SQM),[14,15] COSMOtherm, and empirical models like QSPR in addition to these calculations. We were able to show that this integrated approach delivers results in very good agreement with subsequent experimental validation.[9] However, it does not cover specific salt−solvent interactions in the bulk electrolyte or processes at the electrolyte−electrode interface, though we have taken steps to integrate these features also into our screening strategy.[16] We see our work as a significant step toward rationalizing the search for new electrolyte materials beyond the current state-of-the-art,[17−19] but detailed computational follow-up investigations[20,21] and final experimental validation can clearly not be replaced completely.

Concerning the detailed computational investigation of bulk electrolyte features at the atomic scale, classical or quantum-level "*ab initio*" molecular dynamics (AIMD) simulations as well as quantum chemical calculations of salt−solvent clusters are feasible. In AIMD, the forces are calculated on the fly from electronic structure theory. It is, therefore, possible to determine the structure and spontaneous events such as structural diffusion without having to rely on preparametrized potentials as in force field calculations. Thus, very reliable microscopic insight can be achieved from a given electronic structure method. Due to the lack of computer time, AIMD

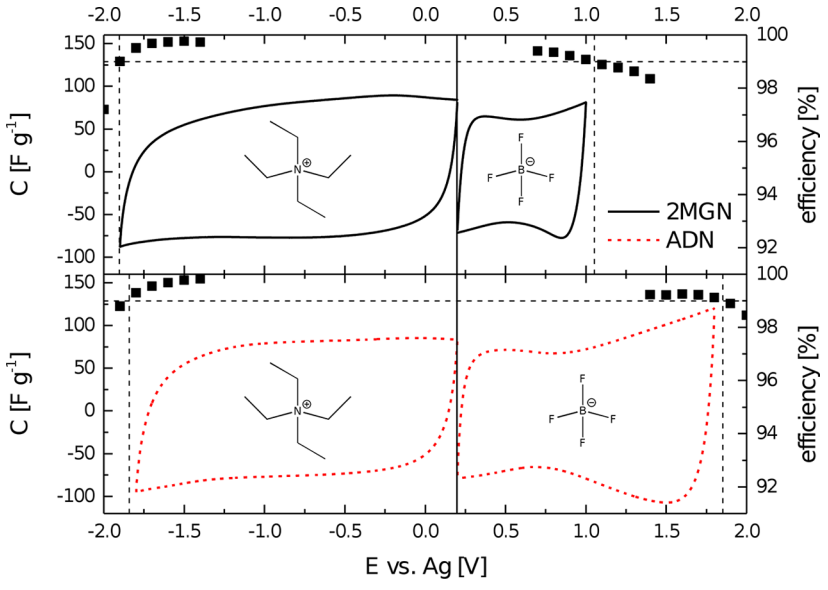

Figure 2. CV measurements for ADN and 2MGN based electrolytes with AC electrodes.

DOI: 10.1021/acs.jpcc.6b00891
J. Phys. Chem. C 2016, 120, 12325−12336

mostly works with dispersion-corrected density functional theory. However, there have been several successful applications ranging from biochemistry to material science.[22]

It has to be kept in mind that even with such sophisticated approaches to treating bulk liquid properties theory is still quite far away from capturing complex interactions at the electrolyte−electrode interface. Interactions responsible for the operative voltage of EDLCs are strongly dependent on the characteristics of the carbonaceous materials, the chemistry of the ions, and experimental conditions. Therefore, accurate prediction of the operative voltage appears challenging to computational investigations.

3. COMPUTATIONAL DETAILS

Born−Oppenheimer molecular dynamics simulations described herein have been carried out within the CP2K[23] program package. In particular, all AIMD calculations were performed with the aid of the QUICKSTEP module,[24] utilizing hybrid Gaussian and plane wave basis sets to calculate the energies and forces on atoms. In this approach, valence electrons are treated in a mixed basis set, with a plane wave energy cutoff equal to 280 Ry and smoothing for the electron density (NN10_SMOOTH) and its derivative (NN10).[24] The molecularly optimized double-ζ basis set (MOLOPT-DZVP-SR-GTH)[25] was used with the effect of core electrons and nuclei considered by using the norm-conserving pseudopotentials of Goedecker−Teter−Hutter.[26−28] The exchange and correlation interactions between electrons were treated with the BLYP functional.[29,30] van der Waals interactions were accounted for by employing empirical corrections prescribed by Grimme.[31]

The systems investigated consist of Et_4NBF_4 surrounded by 64 molecules of the nitrile solvents, illustrated in Figure 3. In order to study ion−solvent interactions in detail, we take two different configurations of the constituent ions in the solvents, placed 5 and 10 Å apart, respectively. We refer to these starting configurations as "associated" and "dissociated" states, denoted A and D henceforth. The starting structures for the AIMD simulations were obtained from classical MD simulations performed, at 300 and 400 K, using the LAMMPS[32] program package. Experimental densities of the nitrile solvents, taken from the literature, were used for the simulations at 300 K. For the simulations at 400 K, preliminary pre-equilibrations were performed for the ion pair in each of the solvents in the constant-NPT ensemble to adjust densities. The values thus obtained were benchmarked against experimentally observed densities. Simulations were performed in the canonical ensemble resulting in over 500 ps of pre-equilibration for each of the investigated systems. The generalized OPLS[33,34] force field was used with partial atomic charges obtained using a restrained electrostatic potential (RESP)[35] fit at the HF 6-31++G** level.[36] The simulation temperatures were set using the Nosé−Hoover thermostat.[37−39]

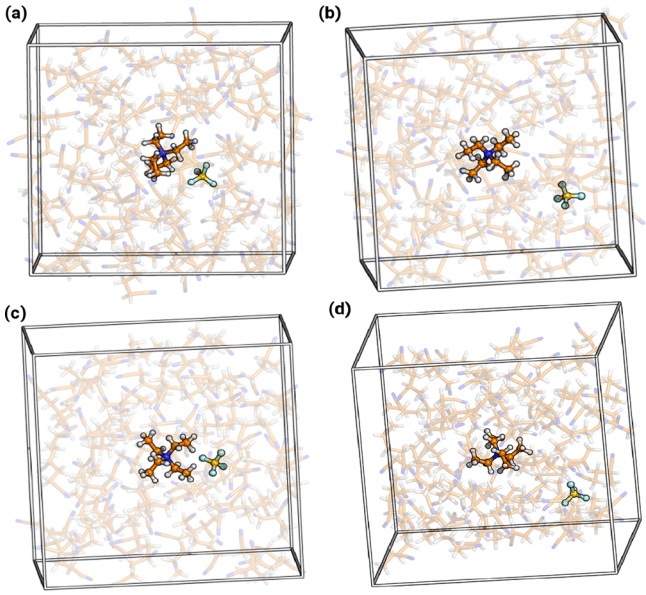

Figure 3. Ball-and-stick representation of the simulated systems. (a) and (b) indicate the associated and dissociated states of ions, respectively, in ADN, while (c) and (d) indicate these states of ions in 2MGN.

Subsequently, AIMD simulations were started, at these temperatures, with the last snapshot of the trajectories obtained from classical MD at the BLYP-D3 level of theory. In each of the simulations, the system was equilibrated for ∼2.5 ps using Nosé−Hoover thermostats for individual atoms with a time constant of 50 fs and a time step of 0.5 fs. The systems were subsequently simulated in the canonical ensemble for 75 ps using a global thermostat. Salt−solvent clusters have been isolated from AIMD runs at both temperatures. The simulations at 400 K are analyzed herein, with the first 10 ps of the production runs excluded from consideration. The validity of AIMD simulations is examined by evaluating the power spectra (Figure S1) of the solvents and subsequent comparison of obtained peaks with the experimental infrared spectra (Supporting Information, Section 1).

The four simulations, detailed above, were, respectively, performed in cubic boxes of the following dimensions: (i) ADN, 400 K: 2466.16 Å, (ii) ADN, 300 K: 2303.33 Å, (iii) 2MGN, 400 K: 2386.53 Å, and (iv) 2MGN, 300 K: 2319.38 Å.

All structure visualization in this work was carried out using the VMD[40] and PyMOL[41] programs. Radial distribution functions (RDFs), angular distribution functions (ADFs), and combined distribution functions (CDFs) are computed with the aid of the TRAVIS[42] program package. Details of trajectory analysis are mentioned in the reference. Occurences of events in the CDFs are illustrated on the RGB scale, shown for each subset of CDFs. Graphical representations were produced with the GRACE program package. CDFs were generated using the GNUPLOT software.

B3LYP[43] calculations for the salt−solvent clusters have been performed with the ORCA[44] program (version 3.0.3) using D3 dispersion corrections,[45] the RI approximation for two-electron integrals,[46] and def2-TZVPP AO basis sets.[47]

4. RESULTS

In the following, we present results from a series of AIMD calculations concerning ions of the salt surrounded by solvent molecules. The resulting trajectories, from the simulations at 400 K, are analyzed to understand important differences in chemical behavior among the considered systems. The following interactions are studied and detailed individually in separate subsections: solvent−solvent, cation−anion, cation−solvent, and anion−solvent. Subsequently, the overall effect of the ions on the considered solvents is investigated. It is important to note that A and D refer to starting configurations, differing solely in the distance between the ions. Nevertheless,

DOI: 10.1021/acs.jpcc.6b00891
J. Phys. Chem. C 2016, 120, 12325−12336

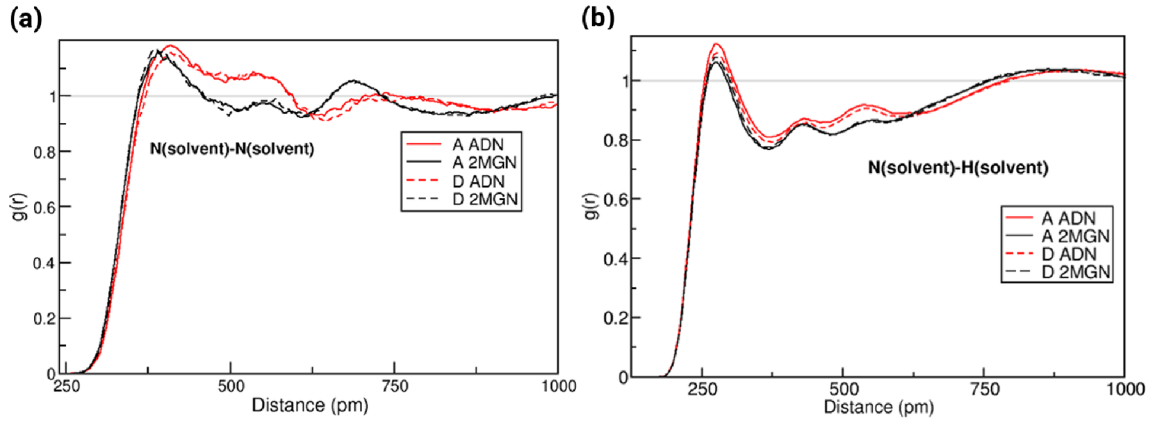

Figure 4. (a) RDFs of the intermolecular N−N distances, suggesting dipole−dipole correlation in the nitrile solvents. (b) RDFs of the intermolecular N−H distances, shown in order to elucidate H bonding in the solvents.

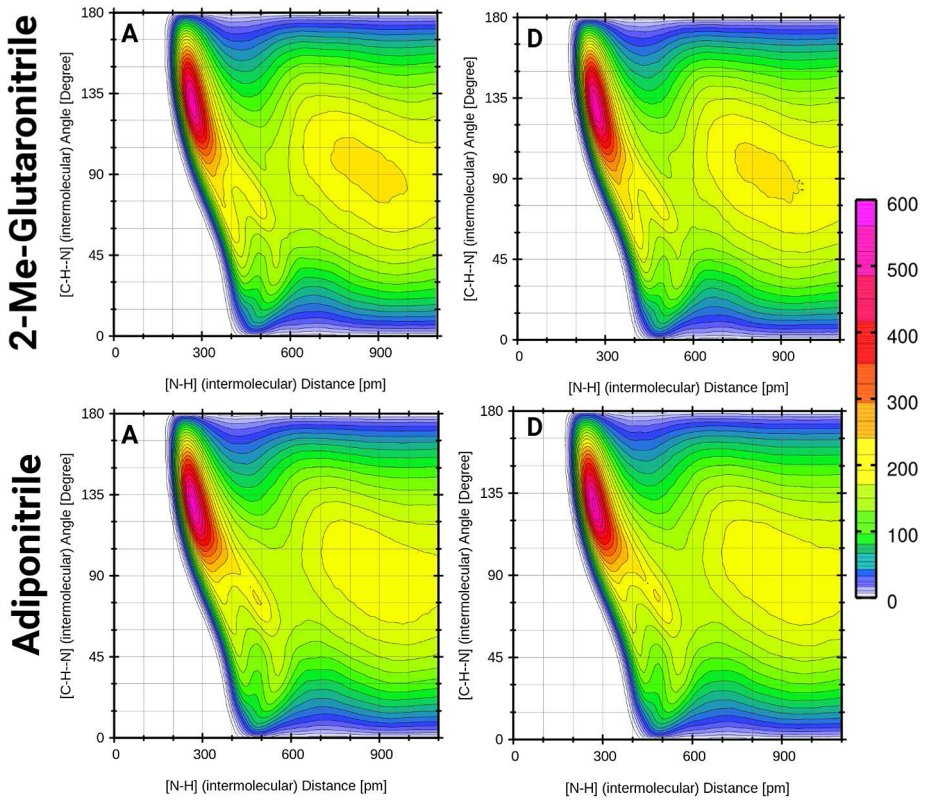

Figure 5. CDFs of the intermolelcular N−H distance along with the C−H−N angle are shown for the four simulations, confirming intermolecular H bonding in the investigated nitrile solvents.

it is noticed that the mean separation between the ions, evaluated for the duration of the simulation, remains similar to that in the starting configuation. Hence, we also present arguments on solvent shells around the respective ions in the discussion herein. However, much longer simulations are required to determine whether these states are preserved in the solvents. Finally, as a second step, we performed DFT calculations on salt−solvent clusters, randomly sampled from the respective AIMD trajectories, to evaluate the electrochemical stability of electrolyte, with a focus on oxidative decomposition.

4.1. Intermolecular Interactions in the Solvent. To elucidate possible solvent−solvent interactions, RDFs corresponding to intermolecular N−N and N−H distances are shown in Figure 4. These distribution functions indicate sufficient convergence with extremely similar appearances for both the solvents.

As expected, the state of the ions introduces no significant change in the solvent−solvent RDFs. A possible dipole−dipole correlation between the solvent molecules can be inferred from the RDFs in Figure 4a. These interactions seem to be slightly stronger and more correlated in 2MGN (black curves in Figure 4a). The directionality is comparatively weaker in ADN (red curves in Figure 4a) with the first peak marginally shifted to the right and the second peak much weaker than in 2MGN. Figure 4b illustrates the possibility of an intermolecular weak C−H···N hydrogen bond between the solvent molecules.

DOI: 10.1021/acs.jpcc.6b00891
J. Phys. Chem. C 2016, 120, 12325−12336

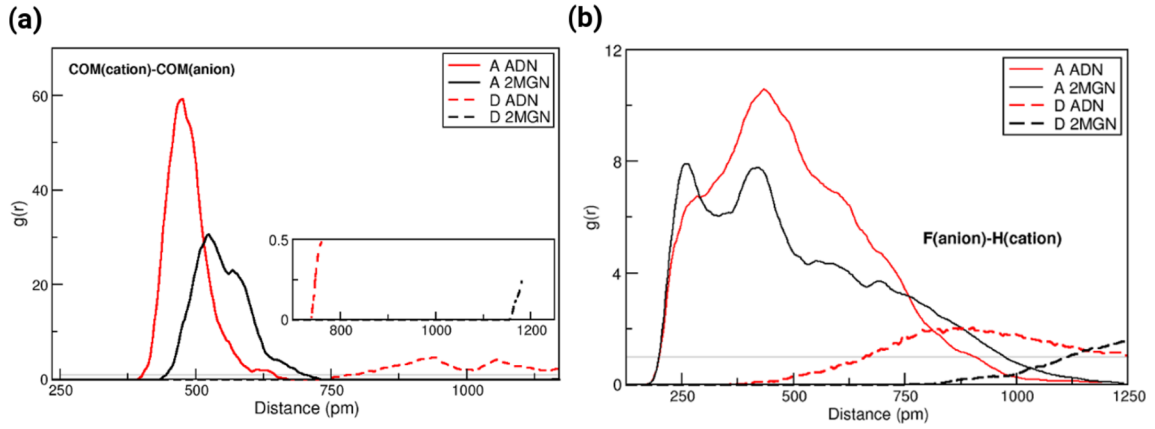

Figure 6. (a) RDFs of the distance between the cation and anion COMs, showing preservation of the dissociated state of ions in 2MGN. Inset shows the RDFs for the dissociated state of ions. (b) RDFs of the distance between F atom and terminal methyl H atoms of the cation illustrating directional, though slightly weaker, H bonding between the associated ions in 2MGN.

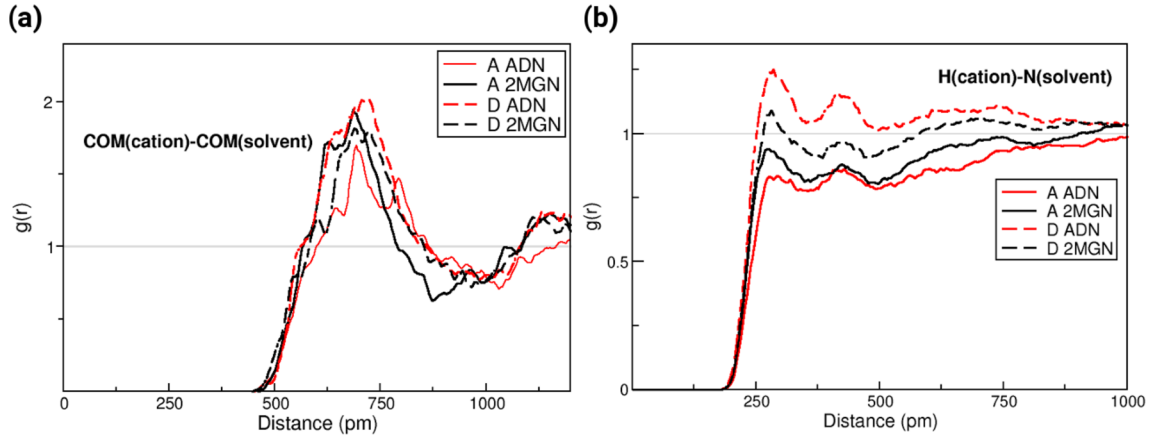

Figure 7. (a) RDFs of the cation−solvent COM distances; largely similar interactions with minor differences between A and D states in ADN. (b) RDFs of the H (cation)−N (solvent) distances, demonstrating strongest H bonding between cation and ADN with the ions separated.

The four RDFs are similar to each other, with ADN showing slightly stronger and more directional hydrogen bonding than 2MGN (red lines in Figure 4b). This is confirmed in the CDFs in Figure 5 where the orientation of solvent molecules with respect to each other is examined. The N−H distance is shown in combination with the C−H···N angle confirming that the peak position in Figure 4b corresponds to weak hydrogen bonding in the solvents and that ADN shows slightly stronger correlation.

4.2. Cation−Anion Interplay. In order to qualitatively understand interactions between the constituent ions of the salt in the two solvents, RDFs corresponding to cation−anion distances are shown in Figure 6. The two considered configurations of the ions are easily distinguishable from the marked peaks compared to the smeared entries at large distances. We consider the distances between the centers of mass (COMs) of the ions in Figure 6a. These RDFs suggest that the ions, in both arrangements, prefer to be more associated in ADN (red curves in Figure 6a) than in 2MGN. The peaks for 2MGN (black curves in Figure 6a), for both states of ions, are less pronounced than in ADN and also at larger distances, noticeably larger than the distance between the ions in the starting configuration. This is particularly significant for the ions separated in 2MGN. The opposite trend is observed for ADN; the ions tend to come slightly closer than in the starting configuration, particularly for the dissociated state. From the presented RDFs, one can loosely define 750 pm as the maximum interionic distance for the ions to be considered "associated" during the course of the simulation. However, cation−anion COM distances, evaluated throughout the trajectory (Figure S2), suggest that interchanging of states is rare, more so in the case of 2MGN, within the duration of the simulation. It has to be pointed out that both sets of simulations indicate preference of ions to be closer together in ADN. Nevertheless, it must be acknowledged that longer simulation time is required to validate these observations. Two states of ions were simulated to capture these effects as large-scale rearrangements of atoms are difficult to be observed within typical AIMD time scales.

In order to understand the orientation of ions around each other, the curves in Figure 6b correspond to distances between F atoms of the anion and the H atoms of the four terminal methyl groups of the cation. The RDFs for the dissociated state again suggest that this state is more preserved in 2MGN (black dashed curve in Figure 6b). However, the RDFs for the associated state cannot be directly related to the ions being loosely bound in 2MGN (black solid curve in Figure 6b) even though the peak for ADN (red solid curve in Figure 6b) is of higher intensity. The first peak of the RDF occurs at a smaller distance in 2MGN than in ADN, indicating more directed

DOI: 10.1021/acs.jpcc.6b00891
J. Phys. Chem. C 2016, 120, 12325−12336

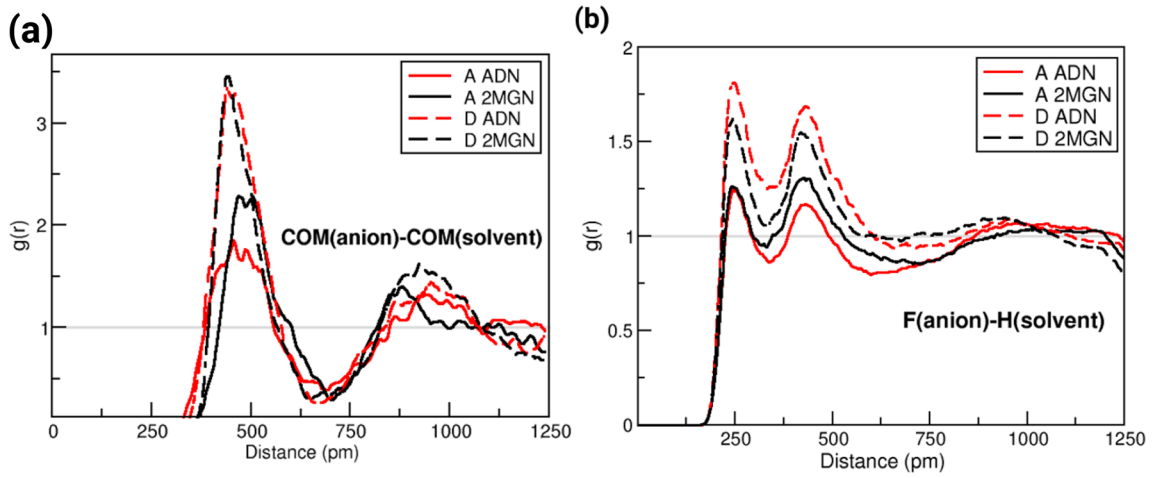

Figure 8. (a) RDFs of the anion−solvent COM distances implying pronounced anion−solvent interactions for dissociated ions. (b) RDFs of the F (anion)−H (solvent) distances showing the strongest anion−solvent H bonding in ADN for the dissociated state.

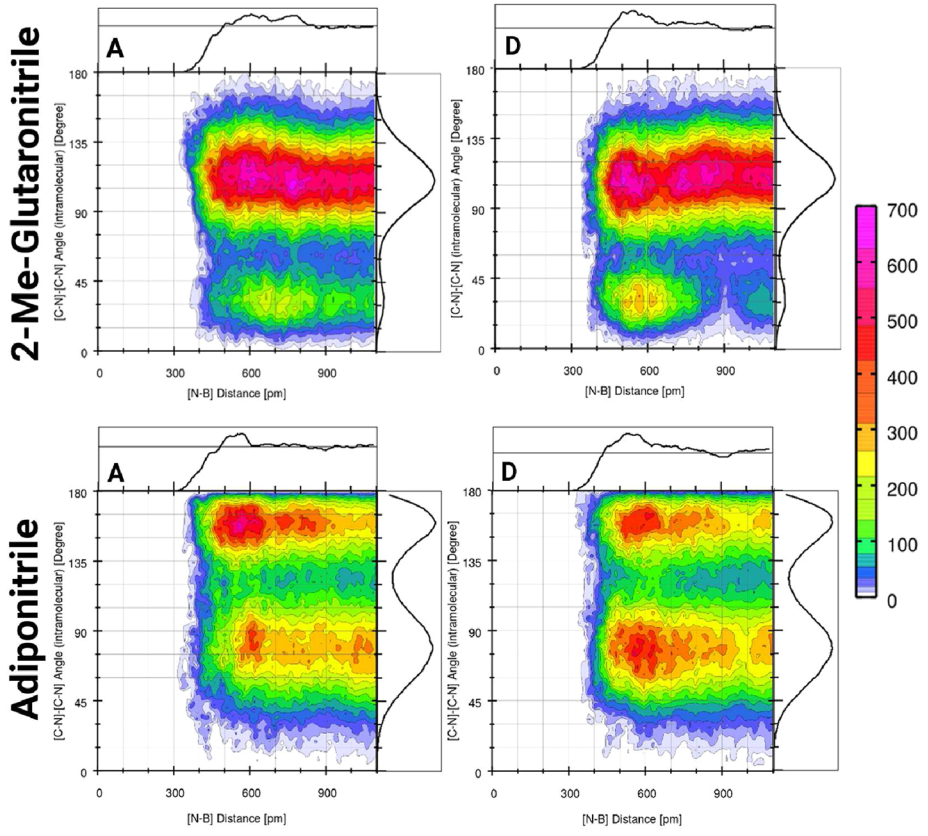

Figure 9. CDFs of the B(anion)−N(solvent) distance in combination with the angle between the intramolecular C−N vectors in the solvent are shown, depicting pronounced correlation between orientation of ADN molecules and proximity of the solvent to the anion.

hydrogen bonding between the anion and cation than in ADN. This could help explain the larger distance between the cation−anion COMs.

4.3. Cation−Solvent Interaction. RDFs corresponding to cation−solvent COM distances shown in Figure 7a suggest extremely similar interactions in all four simulations; peak positions are largely similar to minor differences while comparing solvents. Interestingly, the form of the RDFs seems to be dependent on the state of the ions although these differences are marginal. The highest intensity of the peak is obtained for the ions dissociated in ADN (red dashed curve in Figure 7a) at a slightly larger cation−solvent distance. Overall, it appears that ADN molecules can assume marginally closer distances to the cation than 2MGN (compare red and black curves in Figure 7a). The first minimum of the RDFs occurs at around 900 pm, a distance larger than the cation−anion distance in the associated state but less than that in the dissociated state. This leads us to conclude that there is likely to be one solvent shell around the cation, interposed between the ions, in the dissociated state. As intended, there is only a shared solvent shell around the cation in the associated state of ions.

DOI: 10.1021/acs.jpcc.6b00891
J. Phys. Chem. C 2016, 120, 12325−12336

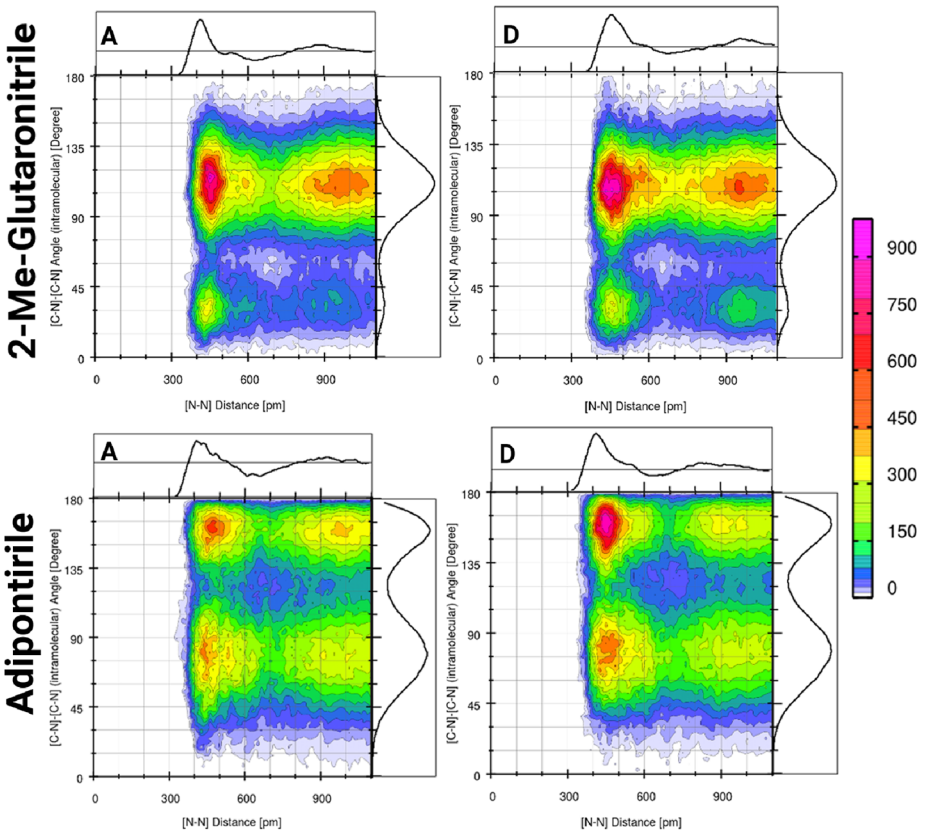

Figure 10. CDFs of the N(cation)−N(solvent) distance in combination with the angle between the intramolecular C−N vectors in the solvent are shown, depicting significant impact of the cation on the orientation of both solvents.

To consider the possibility of hydrogen bonding between the cation and solvent, distances between H atoms of the cation and N atoms of the solvent are shown in Figure 7b. Here, there is a significant difference in the strength of the interactions in the RDFs, for the states of the ions, although the peak positions and features are almost identical. Hydrogen bonding is seen to be the strongest in ADN with the ions in the dissociated state (red dashed curve in Figure 7b) which could explain the higher cation−solvent distances in Figure 7a (red dashed curve). Differences in cation−solvent interactions, for associated and dissociated states of the ions, are more pronounced in ADN (compare red curves, both solid and dashed, against the corresponding black curves).

4.4. Anion−Solvent Interaction. Similarities between anion−solvent and cation−solvent interactions can readily be seen from Figure 8a. ADN can approach the anion marginally closer than 2MGN, and the largest peaks are obtained for the dissociated state of ions in both solvents (red and black dashed curves in Figure 8a). In addition, peak positions are slightly different while comparing solvents, as with the cation−solvent interactions. The state of the ions noticeably influences the shape of the RDFs. An interesting observation here is the pronounced difference between associated and dissociated states of the ions (solid and dashed curves in Figure 8a). This implies that the cation's interaction shell occupies more of the anion's than vice versa. This can be expected based on the difference in the size of the ions. The first minimum of the RDFs occurs around 700 pm which implies the presence of overlapping solvent shells around the cation and anion for the dissociated state of ions. As with the cation−solvent interaction, there is no possibility of a separate solvent shell around the anion when the ions are kept close together.

The hydrogen bonding behavior of the anion with the solvent shown in Figure 8b follows the above-mentioned trend in that there is a large difference between the dissociated and associated state of the ions in terms of peak height (red and black dashed curves in Figure 8b). Also, as in the case of cation−solvent hydrogen bonding, the strongest interactions are observed for the dissociated ions in ADN (red dashed curve in Figure 8b). The four RDFs vary only in peak intensities with identical forms and positions. The double peak structure might be indicative of two types of F atoms or H atoms. The hydrogen bonding of the anion with solvent is much more pronounced than that of the cation with the solvent. As with the cation−solvent interactions, the state of the ions has a more noticeable impact on interactions in ADN than in 2MGN (red solid and red dashed curves against corresponding black curves in Figure 8b).

4.5. Impact on Solvent. In order to understand structural changes in the solvent introduced by the salt, the orientation of the terminal CN groups is studied in combination with distance from the constituent ions. Figure 9 shows the two most probable conformations of ADN: antiparallel and perpendicular arrangements of the C−N vectors with respect to each other. 2MGN also exhibits two conformations, but the vectors are largely aligned antiparallel to each other. Thus, the two solvents show a marked difference with respect to orientation of terminal C−N groups.

CDFs in Figure 9 for 2MGN indicate negligible correlation between the orientation of C−N vectors and solvent−anion distance. In ADN, proximity to the anion generally favors either

DOI: 10.1021/acs.jpcc.6b00891
J. Phys. Chem. C 2016, 120, 12325−12336

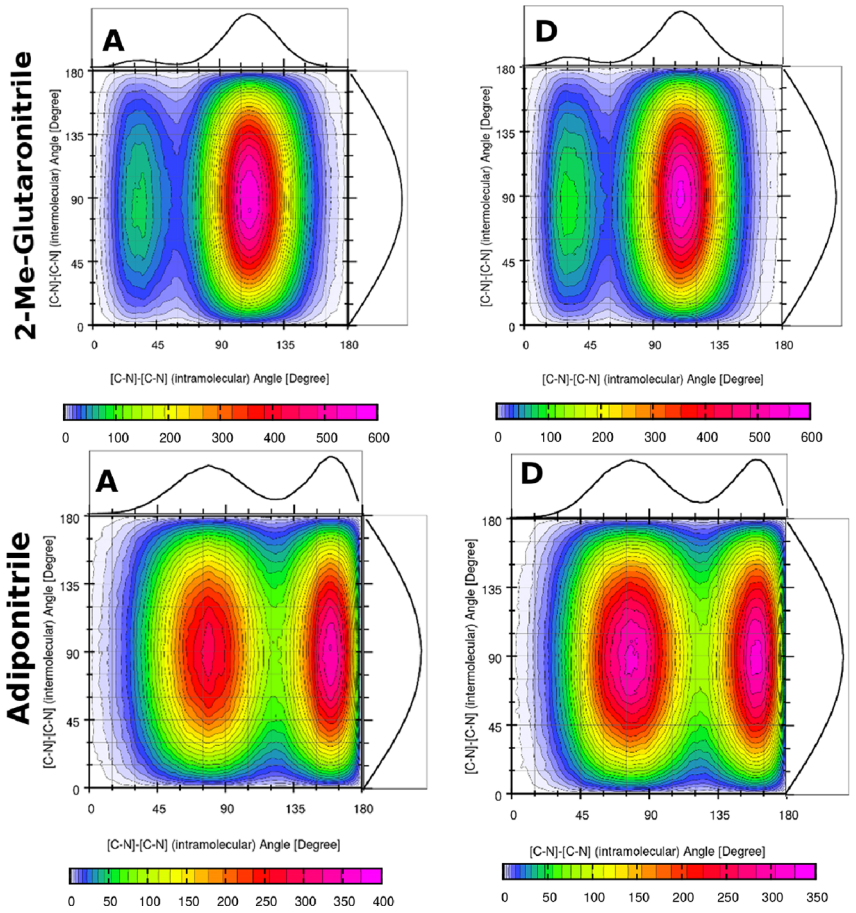

Figure 11. CDFs of the angle between intramolecular C−N vectors and the angle between intermolecular C−N vectors in each of the solvents are shown, illustrating intramolecular and intermolecular conformations of the solvents in the field of the ions.

of the dominant arrangements with a significant shift to the perpendicular arrangement of vectors when the ions are moved apart from each other. This is also observed for 2MGN but much less noticeably. The anion has a larger visible impact on the orientation of ADN than 2MGN, particularly when the ions are dissociated.

Figure 10 suggests pronounced correlation between the cation−solvent distance and the orientation of the relevant vectors. Antiparallel conformations are significant for small distances from the cation although there is a small probability in 2MGN for very large distances as well. For ADN, both the conformations become most probable when the cation is in the immediate vicinity of the solvent, seen more clearly for the dissociated state of ions. However, the antiparallel conformation is more probable. The cation does not induce the perpendicular conformation for either of the solvents in the dissociated state.

We finally investigate the correlation in the angles between intramolecular and intermolecular C−N vectors in Figure 11. The motivation is to check whether perpendicular orientations are also possible intermolecularly in the field of the ions. In fact, the ADFs for both the solvents suggest that intermolecular C−N vectors are largely perpendicular to each other. The CDFs for 2MGN can be expected from earlier observations in that antiparallel conformations within the same molecule will favor perpendicular conformation intermolecularly. However, in ADN, the dissociated state of ions also favors both intermolecular and intramolecular CN vectors oriented perpendicularly to each other. It is observed that the impact of the salt on the solvent seems to be independent of the state of the ions. This further confirms that the results obtained are not limited to particular arrangements of ions around the solvents.

4.6. Bulk Electrolyte Effects on the Electrochemical Stability. The observations thus far can be summarized in the following: intermolecular interactions in ADN seem weaker than in 2MGN, with especially the N−N correlation more directed in the latter case. The ions tend to be more associated in ADN possibly because of different ion−solvent interactions; ADN can approach the ions closer, and the solvent is more structured by the anion's presence. Importantly, differences in how close the solvent can approach the ions between the associated and dissociated states are more pronounced for ADN. This suggests that fewer beneficial solvent−solvent interactions are lost in the case of ion pairing in ADN than 2MGN, if only for purely geometrical reasons. Further investigations are necessary to clarify this. However, the above analyzed data from the AIMD simulations are evidence enough that ion pair formation is a feature that distinguishes ADN from 2MGN based electrolyte solutions. The logical next step, therefore, is to study the effects of ion pair formation on the electrochemical stability of the pure electrolyte.

Electrochemical stability windows can be computed from the corresponding oxidation and reduction potentials, with an additional shift for the chosen reference electrode (7.85 V, in our case).

DOI: 10.1021/acs.jpcc.6b00891
J. Phys. Chem. C 2016, 120, 12325−12336

$$V_{ox} = -\frac{\Delta G_{ox}}{nF} \quad V_{red} = -\frac{\Delta G_{red}}{nF}$$

Redox potentials are in turn computed from free energies of the neutral, oxidized, and reduced molecular species

$$\Delta G_{ox} = \Delta G(X) - \Delta G(X^+)$$
$$\Delta G_{red} = \Delta G(X^-) - \Delta G(X)$$

evaluated from electronic energies with zero-point, thermal enthalpic, entropic, and solvation contributions.

$$\Delta G = \Delta H - T\Delta S = \Delta E + \Delta E_{ZVPE} + \Delta H_T - T\Delta S + \Delta G_{solvation}$$

The latter are commonly taken into account via implicit solvation models. Zero-point vibrational, thermal, enthalpic, and entropic effects usually cancel out to a large extent when computing the difference between neutral and charged states. Therefore, the differences of electronic energies, i.e., the electron affinity (EA) and ioniziation potential (IP), can be used as a rather good estimate for the oxidation and reduction potentials.

$$\Delta G_{ox} \approx \mathrm{IP} = \Delta E_{ox} = E(X) - E(X^+)$$
$$\Delta G_{red} \approx \mathrm{EA} = \Delta E_{red} = E(X^-) - E(X)$$

EAs are more costly to evaluate and often more problematic than IPs, as diffuse basis sets are needed, while medium-sized sets can lead to artifical binding of the additional electron. Tozer and De Proft have discussed this in detail and suggested the following approximation to estimate EAs.[48]

$$\mathrm{EA} = -(E_{LUMO} + E_{HOMO}) - \mathrm{IP}$$

We have found this to work reasonably well for our purposes in the past[12] but provide both calculated as well as estimated values here. The focus of the following analysis is anyhow on the oxidative stability of the salt in the two nitrile solvents and, therefore, on the calculation of IPs.

It is not too obvious how to compute the electrochemical stability of interacting systems (opposed to a single species) in the bulk most efficiently, a fact that was recently discussed by Leung and co-workers.[49] They go through the different options of (a) implicit solvation based cluster model calculations, both with or without solvent molecules in the cluster model, and (b) fully explicit solvent calculations but resort to a mixed explicit/implicit model for their work. Although in principle, (b) comes with less approximations, especially concerning the demarcation of the explicit and implicit solvent regions, the calculation of electrochemical stabilities for the periodic sytem is practically hampered by inaccuracies in the most often used GGA functionals and conceptual difficulties: One can either look at band structures as the equivalent of using orbital eigenvalues (with similar limitations in the accuracy) or compute IPs and EAs in a periodic approach and then correct for the effect of the charged background approximation, which is necessary to keep the periodic cell neutral and which itself can be problematic.[50,51] Mixed explicit/implicit models are very successfully used in computational electrochemistry,[20] though the situation becomes less clear if interacting (salt/solvent or salt/salt) species are investigated. To the best of our knowledge, a systematic assessment of the benefits and drawbacks of the periodic versus the cluster-based approaches for such systems is still missing. We resort here to calculations on cluster models. However, a single cluster does not represent a good model for the liquid phase. Therefore, we attempt to average electrochemical stability estimates over a number of MD snapshots.

Thus, to investigate bulk electrolyte effects on the electrochemical stability in our case, salt−solvent clusters were isolated from the AIMD simulations. All clusters contained the two ions, with either two, three, or six surrounding solvent molecules. Figure 12 shows examples of structures obtained from AIMD trajectories, each including two molecules of respective solvents.

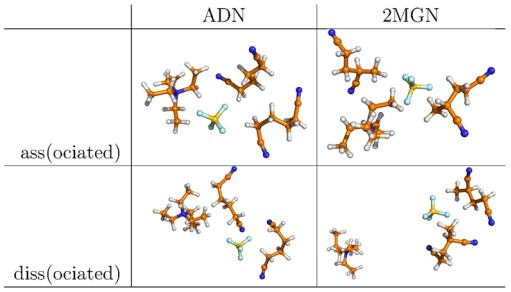

Figure 12. Example structures for the investigated salt/solvent clusters.

Table 1 presents B3LYP-D3/def2-TZVPP level ionization potentials (IPs) and electron affinities (EAs) with and without

Table 1. Averaged Electrochemical Stability Estimates (IPs, EAs) for Randomly Picked Salt/Solvent Clusters from AIMD Simulation Runs at Different Temperatures (300 and 400 K) and with Different Starting Configurations of the Conduction Salt Ions (ass = Associated, diss = Dissociated), as Well as Their Constituent Molecular Species[a]

solvent	start	T	#Ox[c]	#Red[c]	IP/eV	EA/eV[b]
without implicit solvation						
ADN	ass	300	-	-	-	-
ADN	ass	400	31	32	1.63	−0.43
ADN	diss	300	42	16	0.87	−0.44
ADN	diss	400	15	25	0.89	−0.48
2MGN	ass	300	31	26	1.73	−0.45
2MGN	ass	400	14	16	1.64	−0.36
2MGN	diss	300	-	-	-	-
2MGN	diss	400	46	13	0.37	−0.61
with implicit solvation						
ADN	ass	300	-	-	-	-
ADN	ass	400	48	-	0.71	-
ADN	diss	300	64	-	0.70	-
ADN	diss	400	32	-	0.66	-
2MGN	ass	300	48	-	0.83	-
2MGN	ass	400	32	-	0.77	-
2MGN	diss	300	-	-	-	-
2MGN	diss	400	48	-	0.63	-
single species						
ADN	-	-	-	-	3.21	−6.40/-6.02*
2MGN	-	-	-	-	3.25	−6.36/-6.00*
BF4-	-	-	-	-	0.26	−0.71/-2.35*
NEt+	-	-	-	-	7.54	−6.63/-7.38*

[a]Values given relative to Ag/Ag+ (7.85 V). [b]B3LYP-D3/def2-TZVPP(/COSMO) level, * = extrapolated according to Tozer/De Proft. [c]Number of clusters over which averages were taken.

DOI: 10.1021/acs.jpcc.6b00891
J. Phys. Chem. C 2016, 120, 12325−12336

the COSMO solvation model (EPS = 20.7) as estimates of the electrochemical stability of the selected clusters. Values changed little for clusters with varying number of solvent molecules, and therefore, distinct values for these cases are not presented herein. Not all calculations converged because many randomly selected clusters were not the best starting geometries for oxidized or reduced complexes. Nonetheless, the number of clusters over which averaging was possible is, in all cases, above 13 with a maximum of 46 (32 to 64 with COSMO). No significant influence was found on changing the number of clusters included for averaging. While IPs are straightforward to calculate, EAs suffer from strong basis set effects (see above for details). Therefore, we provide extrapolated values for the separated molecular species instead of using augmented basis sets. Since the reductive stability is not of prime importance in the problem considered here, this approach seems reasonable. Experimentally measured stabilities are given relative to a reference potential of Ag/Ag+ here, calculated to be 7.85 V at the B3LYP-D3/def2-TZVPP level, and this value is accordingly subtracted from all computed potentials to arrive at the values in Table 1. If we subtract this from the highest IP value for single separated molecular species (8.11 V for BF4−) and the corresponding lowest extrapolated EA value (5.50 V for BF4−), we arrive at a first, rough estimate of the electrochemical stability windows for the pure electrolyte, i.e., −2.35 to 0.26 V.

From Table 1, one finds that the electrochemical stability against reduction varies little between all investigated clusters and seems to be dominated by the stability of the anion. This is rather unintuitive and clearly merits further investigation but is beyond the scope of the discussion presented here, as we aim at understanding the different operative voltages with ADN and 2MGN based electrolytes that result from a substantially lower oxidative stability of the latter. Oxidative stabilities are given without and with implicit solvation. Without implicit solvation, the oxidative stability does not vary between clusters from AIMD runs at different temperatures and again seems to be dominated by anion stability. However, a strong effect is found for the association of the ions, for both ADN as well as 2MGN. Solvation (cluster formation) increases the oxidative stability of the electrolyte by about 0.6 V for ADN and 0.1 V for 2MGN, whereby the lower value for 2MGN has to be attributed to more associated clusters, even for the dissociated AIMD runs. The resulting electrochemical stability window of about 3.2 V (−2.35 to 0.86 V) would be in good agreement with experiment for 2MGN (2.95 V). In the case of ADN, the experimental value of 3.70 V is much closer to the one obtained with ions paired, which is again about 0.8 V higher, summing up to about 4.0 V (−2.35 to 1.63 V) overall. Apart from looking at average values, we also investigated the correlation of the fluctuation of the values. Correlation factors are very low between −0.24 and +0.37, with a value of 0.60 in just one case, and standard deviations were small with values from ±0.14 to ±0.24 eV. Both measures thus indicate no systematic differences beyond those found for the averages. The increased electrochemical stability of the ion pair can probably be attributed to a charge transfer between the ions in the associated state, which has been shown to be large enough for similar ions.[52] We plan to investigate this in more detail within our studies on the interplay of the bulk electrolyte with the electrode surface. Interestingly, we did not find substantial changes when including more (2 to 6) solvent molecules into the cluster model. However, using implicit solvation changes the picture significantly, in that a much more similar oxidative stability is found for the associated and dissociated states. These two findings seem rather contradictory to us. One possibility is that the shielding between the ions is too perfect with the implicit model, in which the accessibility of the ions by the solvent molecules is not accounted for correctly. It is hard to draw any definite conclusions from this, but the message seems to be that the observed differences can only play a role in the case of imperfect solvation, for instance upon partial solvent stripping at the electrode surface.

Our cluster based calculations, therefore, seem to be able to explain the observed difference of 0.75 V (0.8 V calculated) but only if ion pairing is assumed to play a more important role in ADN than 2MGN. Ion pairs are generally assumed to be present to some extent in organic liquid based electrolytes, but it seems questionable that the difference in the concentration of ion pairs in ADN and 2MGN bulk electrolytes should be large enough to explain our problem. Keeping in mind the above-mentioned finding, that charging at the positively polarized electrode proceeds via the exchange of cations for anions, it seems natural to assume that the different ion pair formation features of ADN and 2MGN play a substantial role in this ion exchange.

CONCLUSIONS

As a preliminary step toward understanding experimentally observed operative voltages in EDLC devices, we conducted AIMD and static, cluster-based quantum chemical investigations of ADN versus 2MGN based EDLC electrolytes. Our simulations indicate that small structural differences of the two nitrile solvents lead to surprisingly large effects on the bulk solvation of the conducting salt in terms of ion pair formation. Additional static calculations show that ion pair formation can lead to an increase in the electrochemical stability of the electrolyte which is similar in size to the experimentally observed, rather large difference between the operative voltages. Such ion association processes are likely to play a role in the ion exchange process taking place upon charging EDLCs. This suggests that our findings explain the bulk electrolyte aspect of the problem although the electrolyte−electrode interface requires further investigation.

ASSOCIATED CONTENT

Supporting Information

The Supporting Information is available free of charge on the ACS Publications website at DOI: 10.1021/acs.jpcc.6b00891.

Table S1 and Figures S1−S2, containing simulated spectra and additional analysis from the AIMD production runs (PDF)

AUTHOR INFORMATION

Corresponding Author

*E-mail: martin.korth@uni-ulm.de.

Notes

The authors declare no competing financial interest.

ACKNOWLEDGMENTS

BK and PR would like to thank the support from the Deutsche Forschungsgemeinschaft under the KI786/8-1 project and the SPP 1708 project KI768/12-1. AB and CS would like to thank the Bundesministerium für Bildung and Forschung (BMBF) within the project IES (contract number 03EK3010) for the financial support. MK, SD, and TH gratefully acknowledge

DOI: 10.1021/acs.jpcc.6b00891
J. Phys. Chem. C 2016, 120, 12325−12336

financial support from the Barbara Mez-Starck Foundation and the DFG Research Unit FOR1376. KAP was funded by the Joint Center of Energy Storage Research (JCESR) an Energy Innovation Hub funded by the U.S. Department of Energy, Office of Basic Energy Sciences, under contract No. DE-AC02-05CH11231. This research was supported in part by the bwHPC initiative and the bwHPC-C5 project through compute services of the JUSTUS HPC facility at the University of Ulm. bwHPC and bwHPC-C5 (http://www.bwhpc-c5.de) are funded by the Ministry of Science, Research and the Arts Baden-Württemberg (MWK), and the Germany Research Foundation (DFG).

REFERENCES

(1) Pandolfo, A. G.; Hollenkamp, A. F. Carbon Properties and Their Role in Supercapacitors. *J. Power Sources* **2006**, *157*, 11−27.
(2) Simon, P.; Gogotsi, Y. Materials for Electrochemical Capacitors. *Nat. Mater.* **2008**, *7*, 845−854.
(3) Ruch, P. W.; Cericola, D.; Foelske, A.; Kotz, R.; Wokaun, A. A Comparison of the Aging of Electrochemical Double Layer Capacitors with Acetonitrile and Propylene Carbonate-Based Electrolytes at Elevated Voltages. *Electrochim. Acta* **2010**, *55*, 2352−2357.
(4) Ruch, P. W.; Cericola, D.; Foelske-Schmitz, A.; Kotz, R.; Wokaun, A. Aging of Electrochemical Double Layer Capacitors with Acetonitrile-Based Electrolyte at Elevated Voltages. *Electrochim. Acta* **2010**, *55*, 4412−4420.
(5) Béguin, F.; Frackowiak, E. *Supercapacitors Materials, Systems, and Applications*; Wiley-VCH: Weinheim, 2013.
(6) Azais, P.; Duclaux, L.; Florian, P.; Massiot, D.; Lillo-Rodenas, M. A.; Linares-Solano, A.; Peres, J. P.; Jehoulet, C.; Beguin, F. Causes of Supercapacitors Ageing in Organic Electrolyte. *J. Power Sources* **2007**, *171*, 1046−1053.
(7) Conte, M. Supercapacitors Technical Requirements for New Applications. *Fuel Cells* **2010**, *10*, 806−818.
(8) Miller, J. R.; Burke, A. F. Electrochemical Capacitors: Challenges and Opportunities for Real-World Applications. *Electrochem. Soc. Interface* **2008**, *17*, 53−57.
(9) Schütter, C.; Husch, T.; Korth, M.; Balducci, A. Toward new solvents for EDLCs: From computational screening to electrochemical validation. *J. Phys. Chem. C* **2015**, *119*, 13413−13424.
(10) Griffin, J. M.; Forse, A. C.; Tsai, W.-Y.; Taberna, P.-L.; Simon, P.; Grey, C. P. n situ NMR and electrochemical quartz crystal microbalance techniques reveal the structure of the electrical double layer in supercapacitors. *Nat. Mater.* **2015**, *14*, 812−819.
(11) Rajput, N. N.; Qu, X.; Sa, N.; Burrell, A. K.; Persson, K. A. The Coupling between Stability and Ion Pair Formation in Magnesium Electrolytes from First-Principles Quantum Mechanics and Classical Molecular Dynamics. *J. Am. Chem. Soc.* **2015**, *137*, 3411−3420.
(12) Korth, M. Large-scale virtual high-throughput screening for the identification of new battery electrolyte solvents: evaluation of electronic structure theory methods. *Phys. Chem. Chem. Phys.* **2014**, *16*, 7919−7926.
(13) Husch, T.; Yilmazer, N. D.; Balducci, A.; Korth, M. Large-scale virtual high-throughput screening for the identification of new battery electrolyte solvents: computing infrastructure and collective properties. *Phys. Chem. Chem. Phys.* **2015**, *17*, 3394−3401.
(14) Korth, M. Third-generation Hydrogen-bonding Corrections for Semiempirical QM Methods and Force Fields. *J. Chem. Theory Comput.* **2010**, *6*, 3808−3816.
(15) Yilmazer, N. D.; Korth, M. Enhanced semiempirical quantum-mechanical methods for biomolecular interactions. *Comput. Struct. Biotechnol. J.* **2015**, *13*, 169−175.
(16) Husch, T.; Korth, M. How to estimate solid-electrolyte-interphase features when screening electrolyte materials. *Phys. Chem. Chem. Phys.* **2015**, *17*, 22799−22808.
(17) Cheng, L.; Assary, R. S.; Qu, X.; Jain, A.; Ong, S. P.; Rajput, N. N.; Persson, K.; Curtiss, L. A. Accelerating Electrolyte Discovery for Energy Storage with High-Throughput Screening. *J. Phys. Chem. Lett.* **2015**, *6*, 283−291.
(18) Borodin, O.; Olguin, M.; Spear, C. E.; Leiter, K. W.; Knap, J. Towards high throughput screening of electrochemical stability of battery electrolytes. *Nanotechnology* **2015**, *26*, 354003.
(19) Husch, T.; Korth, M. Charting the known chemical space for non-aqueous Lithium-air battery electrolyte solvents. *Phys. Chem. Chem. Phys.* **2015**, *17*, 22596−22603.
(20) Korth, M. In *Chemical Modeling*; Springborg, M., J.-O, J., Ed.; Royal Society of Chemistry: London, 2015; Vol. *11*, p 57.
(21) Korth, M.; Grimme, S.; Towler, M. D. The Lithium-thiophene Riddle Revisited. *J. Phys. Chem. A* **2010**, *115*, 11734−11739.
(22) Kirchner, B.; Dio, P.; Hutter, J. In *Multiscale Molecular Methods in Applied Chemistry*; Kirchner, B., Vrabec, J., Eds.; Topics in Current Chemistry; Springer: Berlin Heidelberg, 2012; Vol. *307*; pp 109−153.
(23) Hutter, J.; Iannuzzi, M.; Schiffmann, F.; VandeVondele, J. cp2k: atomistic simulations of condensed matter systems. *Wiley Interdiscip. Rev.: Comput. Mol. Sci.* **2014**, *4*, 15−25.
(24) VandeVondele, J.; Krack, M.; Mohamed, F.; Parrinello, M.; Chassaing, T.; Hutter, J. QUICKSTEP: Fast and Accurate Density Functional Calculations Using a Mixed Gaussian and Plane Waves Approach. *Comput. Phys. Commun.* **2005**, *167*, 103−128.
(25) VandeVondele, J.; Hutter, J. Gaussian Basis Sets for Accurate Calculations on Molecular Systems in Gas and Condensed Phases. *J. Chem. Phys.* **2007**, *127*, 114105.
(26) Goedecker, S.; Teter, M.; Hutter, J. Separable Dual-Space Gaussian Pseudopotentials. *Phys. Rev. B: Condens. Matter Mater. Phys.* **1996**, *54*, 1703−1710.
(27) Hartwigsen, C.; Goedecker, S.; Hutter, J. Relativistic Separable Dual-Space Gaussian Pseudopotentials from H to Rn. *Phys. Rev. B: Condens. Matter Mater. Phys.* **1998**, *58*, 3641−3662.
(28) Krack, M. Pseudopotentials for H to Kr Optimized for Gradient-Corrected Exchange-Correlation Functionals. *Theor. Chem. Acc.* **2005**, *114*, 145−152.
(29) Becke, A. Density-functional exchange-energy approximation with correct asymptotic-behavior. *Phys. Rev. A: At., Mol., Opt. Phys.* **1988**, *38*, 3098−3100.
(30) Lee, C.; Yang, W.; Parr, R. G. Development of the Colle-Salvetti correlation-energy formula into a functional of the electron density. *Phys. Rev. B: Condens. Matter Mater. Phys.* **1988**, *37*, 785−789.
(31) Grimme, S.; Antony, J.; Ehrlich, S.; Krieg, H. A Consistent and Accurate ab initio Parametrization of Density Functional Dispersion Correction (DFT-D) for the 94 Elements H-Pu. *J. Chem. Phys.* **2010**, *132*, 154104.
(32) Plimpton, S. Fast Parallel Algorithms for Short-Range Molecular Dynamics. *J. Comput. Phys.* **1995**, *117*, 1−19.
(33) Jorgensen, W. L.; Maxwell, D. S.; Tirado-Rives, J. Development and testing of the OPLS all-atom force field on conformational energetics and properties of organic liquids. *J. Am. Chem. Soc.* **1996**, *118*, 11225−11236.
(34) Kaminski, G.; Jorgensen, W. L. Performance of the AMBER94, MMFF94, and OPLS-AA force fields for modeling organic liquids. *J. Phys. Chem.* **1996**, *100*, 18010−18013.
(35) Singh, U. C.; Kollman, P. A. An approach to computing electrostatic charges for molecules. *J. Comput. Chem.* **1984**, *5*, 129−145.
(36) Hehre, W. J.; Ditchfield, R.; Pople, J. A. Self-consistent molecular orbital methods. XII. Further extensions of gaussian type basis sets for use in molecular orbital studies of organic molecules. *J. Chem. Phys.* **1972**, *56*, 2257−2261.
(37) Nosé, S. A unified formulation of the constant temperature molecular-dynamics methods. *J. Chem. Phys.* **1984**, *81*, 511−519.
(38) Hoover, W. G. Canonical Dynamics - Equilibrium Phase-Space Distributions. *Phys. Rev. A: At., Mol., Opt. Phys.* **1985**, *31*, 1695−1697.
(39) Martyna, G. J.; Klein, M. L.; Tuckerman, M. Nosé-Hoover Chains: The Canonical Ensemble Via Continuous Dynamics. *J. Chem. Phys.* **1992**, *97*, 2635−2643.
(40) Humphrey, W.; Dalke, A.; Schulten, K. VMD − Visual Molecular Dynamics. *J. Mol. Graphics* **1996**, *14*, 33−38.

DOI: 10.1021/acs.jpcc.6b00891
J. Phys. Chem. C 2016, 120, 12325−12336

(41) DeLano, W. L. Pymol: An open-source molecular graphics tool. *CCP4 Newsletter On Protein Crystallography* **2002**, *40*, 82−92.
(42) Brehm, M.; Kirchner, B. TRAVIS-a free analyzer and visualizer for Monte Carlo and molecular dynamics trajectories. *J. Chem. Inf. Model.* **2011**, *51*, 2007−2023.
(43) Stephens, P. J.; Devlin, F. J.; Chabalowski, C. F.; Frisch, M. J. Ab Initio Calculation of Vibrational Absorption and Circular Dichroism Spectra Using Density Functional Force Fields. *J. Phys. Chem.* **1994**, *98*, 11623−11627.
(44) Neese, F. The ORCA program system. *Wiley Interdiscip. Rev.: Comput. Mol. Sci.* **2012**, *2*, 73−78.
(45) Grimme, S.; Antony, J.; Ehrlich, S.; Krieg, H. *J. Chem. Phys.* **2010**, *132*, 154104.
(46) Eichkorn, K.; Weigend, F.; Treutler, O.; Ahlrichs, R. Auxiliary basis sets for main row atoms and transition metals and their use to approximate Coulomb potentials. *Theor. Chem. Acc.* **1997**, *97*, 119−124.
(47) Schäfer, A.; Huber, C.; Ahlrichs, R. Fully optimized contracted Gaussian basis sets of triple zeta valence quality for atoms Li to Kr. *J. Chem. Phys.* **1994**, *100*, 5829−5835.
(48) Tozer, D. J.; De Proft, F. Computation of the hardness and the problem of negative electron affinities in density functional theory. *J. Phys. Chem. A* **2005**, *109*, 8923−8929.
(49) Leung, K.; Chaudhari, M. I.; Rempe, S. B.; Fenton, K. R.; Pratt, H. D.; Staiger, C. L.; Nagasubramanian, G. Density Functional Theory and Conductivity Studies of Boron-Based Anion Receptors. *J. Electrochem. Soc.* **2015**, *162*, A1927−A1934.
(50) Lozovoi, A.; Alavi, A.; Kohanoff, J.; Lynden-Bell, R. Ab initio simulation of charged slabs at constant chemical potential. *J. Chem. Phys.* **2001**, *115*, 1661−1669.
(51) Hub, J. S.; de Groot, B. L.; Grubmúller, H.; Groenhof, G. Quantifying artifacts in Ewald simulations of inhomogeneous systems with a net charge. *J. Chem. Theory Comput.* **2014**, *10*, 381−390.
(52) Kirchner, B.; Malberg, F.; Firaha, D. S.; Hollóczki, O. Ion pairing in ionic liquids. *J. Phys.: Condens. Matter* **2015**, *27*, 463002.

DOI: 10.1021/acs.jpcc.6b00891
J. Phys. Chem. C 2016, 120, 12325−12336